From quantum to classical images

A. Gatti and L.A. Lugiato

Istituto Nazionale di Fisica per la Materia, Dipartimento Di Fisica,
Via Celoria 16, 20133 Milano, Italy

lugiato@mi.infn.it

Gian–Luca Oppo and Richard Martin

Department of Physics, University of Strathclyde,
107 Rottenrow, Glasgow G4 ONG, Scotland

gianluca@phys.strath.ac.uk

P. Di Trapani

Istituto di Scienze Matematiche, Fisiche e Chimiche, and Istituto Nazionale di
Fisica per la Materia, Università di Milano, sede di Como,
Via Lucini 3, 22100 Como, Italy

ditrapani@fis.unico.it

and A. Berzanskis[1]

Faculty of Physics and Medical Engineering, Technical University of Jena,
Tateendpromenade 16, D - 07745 Jena, Germany

audrius@stud.fh-jena.de

Abstract: We display the results of the numerical simulations of a set of Langevin equations, which describe the dynamics of a degenerate optical parametric oscillator in the Wigner representation. The scan of the threshold region shows the gradual transformation of a quantum image into a classical roll pattern. An experiment on parametric down–conversion in lithium triborate shows strikingly similar results in both the near and the far field, displaying qualitatively the classical features of quantum images.

OCIS codes: (190.4420) Nonlinear optics, transverse effects in, (270.2500) Fluctuations, relaxations, and noise

References

1. H. Haken, " Synergetics - An introduction" (Springer–Verlag, Berlin 1977)
2. G. Nicolis and I. Prigogine, "Self Organization in Nonequilibrium Systems" (Wiley, New York 1977)
3. L.A. Lugiato ed., Special Issue on "Nonlinear Optical Structures, Pattern, Chaos", Chaos Solitons and Fractals, August/September 1994
4. A. Gatti and L.A. Lugiato, "Quantum Images and Critical Fluctuations in the Optical Parametric Oscillator Below Threshold", Phys. Rev. A **52**, 1675 (1995)
5. A. Gatti, H. Wiedemann, L.A. Lugiato, I. Marzoli, G.-L. Oppo and S.M. Barnett , "Langevin treatment of quantum fluctuations and optical patterns in optical parametric oscillators below threshold", Phys. Rev. A, in press (July 1997)
6. I. Marzoli, A. Gatti, and L.A. Lugiato, "Spatial quantum signatures in parametric downconversion", Phys. Rev. Lett. **78**, 2092 (1997)

#1968 - $10.00 US Received June 25, 1997; Revised July 2, 1997

7. P.D. Drummond, K.J. McNeil, and D.F. Walls, "Non-equilibrium transitions in sub/second harmonic generation", Optica Acta **27**, 321 (1980); "Non-equilibrium transitions in sub/second harmonic generation. II. Quantum theory", Optica Acta **28**, 211 (1981)

8. G.–L. Oppo, M. Brambilla, and L.A. Lugiato, "Formation and evolution of rolls pattern in optical parametric oscillators", Phys. Rev A **49**, 2028 (1994)

9. L. A. Lugiato and A. Gatti, "Spatial Structure of a Squeezed vacuum", Phys. Rev. Lett. **70**, 3868 (1993)

10. E.M. Nagasako, R.W. Boyd, and G.B. Agarwal, "Vacuum field induced filamentation in laser beam propagation", Phys. Rev. A **55**, 1412 (1997)

11. S.X. Dou, D. Josse, and J. Zyss, "Comparison of collinear and one-beam noncollinear phase matching in optical parametric amplification", J. Opt. Soc. Am B 9, 1312 (1992)

12. P. Di Trapani, A. Andreoni, G. P. Banfi, C. Solcia, R. Danielius, P. Foggi, M. Monguzzi, A. Piskarskas and C. Sozzi, "Group-velocity self-matching of femtosecond pulses in non-collinear parametric generation", Phys. Rev. A 51, 3164 (1995)

1. Introduction

Most fascinating in Science is the general phenomenon of spontaneous formation of spatial pattern from a homogeneous background, when a control parameter, say β, is raised to the critical value β_c, where the pattern formation starts [1,2]. For a 2D system with translational and rotational symmetry, the analysis is best carried out in terms of the spatial Fourier transform of the field in play. The instability which leads to pattern formation develops over a critical circle of radius k_c in the Fourier plane. When the control parameter β is slightly larger than β_c small perturbations of the form $\exp(\mathrm{i}\vec{k}\cdot\vec{x})$, where $\vec{k}=(k_x,k_y)$, $\vec{x}=(x,y)$, with $|\vec{k}|=k_c$, do not decay in time, but grow and give rise to a spatial structure. Usually the system breaks spontaneously also the rotational symmetry and only a small set of points on the circle $|\vec{k}|=k_c$ contribute to the final pattern. If, for example, only two vectors $\vec{k}$ and $-\vec{k}$ contribute to the pattern with equal weight, the combination of $\exp(\mathrm{i}\vec{k}\cdot\vec{x})$ and $\exp(-\mathrm{i}\vec{k}\cdot\vec{x})$ gives rise to a roll structure. In general, the selection of the final pattern is governed by the nonlinearity with the constraint of conservation of the total wave vector.

When the control parameter β is smaller than but close enough to β_c, the onset of a spatial structure is heralded by the spatial correlation function, which exhibits a modulation with a wavelength $2\pi/k_c$ [2].

In the case of nonlinear optical systems, the spatial Fourier transform corresponds to the "far field" configuration of the field itself. The law of conservation of total wave vector is what is usually called the phase matching condition in nonlinear optics. [2] Most important of all, nonlinear optical structures are capable of displaying relevant quantum features, even at room temperature. The main reason for this is that the interaction processes which give rise to pattern formation in optics, correspond to simultaneous destruction and creation of photons, and this circumstance creates correlations of quantum nature.

If, for example, a degenerate optical parametric oscillator (OPO) below threshold is considered, the control parameter is the input field amplitude, and the critical point β_c corresponds to the threshold for signal generation. Below threshold, according to the semiclassical picture, the signal field is exactly zero. On the other hand, in a fully quantum description, due to the presence of quantum noise, the signal field is zero only on average and on approaching threshold it shows a spatial modulation, basically with a

[2]For a general introduction on the field of optical pattern formation, see *e.g.* [3] and references quoted therein.

#1968 - $10.00 US Received June 25, 1997; Revised July 2, 1997

wavelength $2\pi/k_c$, with a noteworthy level of spatial order. We use the name "quantum image" [4–5] to designate these noisy field configurations generated by quantum fluctuations. The analysis of spatial correlations in the far field shows clear signatures of the quantum nature of the fluctuations that create the image [6, 5]. In this paper we show in detail the scan of the threshold region of the OPO, with a gradual transformation of the quantum image to a classical image (the roll pattern).

In addition we describe an experiment, performed in the laboratories of the Como branch of Milano University, which studies the propagation of a pump field along a sample of $\chi^{(2)}$ material. The pump field generates a signal and an idler field at lower frequencies, via a process of parametric down conversion induced by quantum fluctuations. The signal field is detected by means of a CCD camera, in the near and in the far field; in both cases the field spatial distribution is closely similar to that shown by our previous numerical results. Despite differences between the experimental setting and the theoretical model studied here, the basic physical mechanisms which give rise to the patterns are closely similar, and this can well explain the impressive similarity of the pictures.

2. The Langevin equation model in the Wigner representation

Let us consider (Fig. 1) a cavity with plane mirrors, containing a medium with a $\chi^{(2)}$ nonlinearity. Mirror M_1 has high reflectivity, while mirror M_2 is completely reflecting, so that the cavity is one-ended. A coherent and stationary field $E_{\rm in}$ of frequency $2\omega_s$ and with a plane wave configuration is injected into the cavity. The output is formed by a field with the same frequency as the input field and, if the pump intensity overcomes a suitable critical value which is the threshold for the optical parametric oscillator, by another field, named the signal field, with frequency ω_s. The generation of the signal field occurs via a process of parametric down-conversion, in which photons of the pump field are converted into pairs of photons of the signal field.

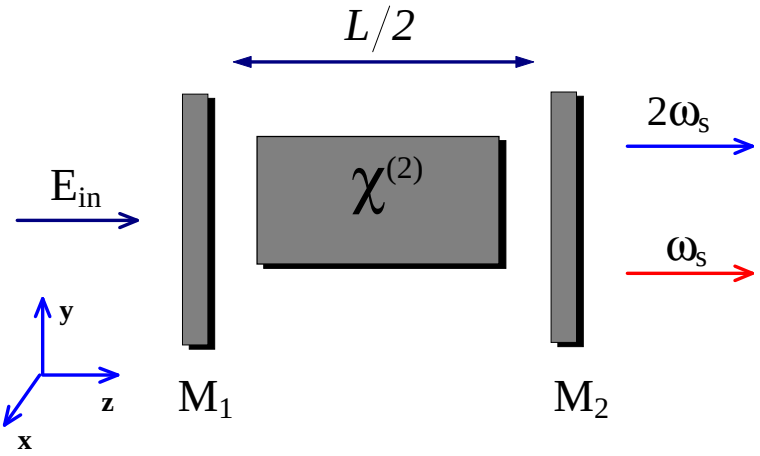

Fig. 1. Scheme of the OPO cavity. The mirror M_1 has a high reflectivity, M_2 is completely reflecting. $E_{\rm in}$ is the input field of frequency $2\omega_s$.

Our model is formulated in terms of Langevin equations for the field distributions $A_0(\vec{x},t)$ and $A_1(\vec{x},t)$ associated with the pump of frequency $2\omega_s$, and with the signal of frequency ω_s, respectively. More precisely, by A_0 and A_1 we indicate the slowly varying envelopes of the pump field and of the signal field. They depend only on time and on the transverse coordinate $\vec{x}=(x,y)$, while the dependence on the longitudinal

#1968 - $10.00 US
Received June 25, 1997; Revised July 2, 1997

coordinate z has been eliminated by assuming the uniform field approximation, so that only one longitudinal cavity mode is relevant for both the pump and the signal field.

The starting point of the model is the master equation for the density operator of the system, which generalizes the standard description of Drummond, McNeil and Walls [8] to include the spatial degrees of freedom. Using the Wigner representation, this master equation is translated into a generalized Fokker–Planck equation for the Wigner functional[5]. This equation includes also terms with third order functional derivatives, which are neglected. Using Ito rules the Fokker–Planck equation obtained in this way is finally translated into classical looking Langevin equations for the scaled fields envelopes A_0, A_1, which read:

$$\begin{aligned}\frac{\partial}{\partial t}A_0(\vec{x},t) &= \gamma_0\left[-\left(1+\mathrm{i}\Delta_0-\mathrm{i}\frac{\gamma_1}{2\gamma_0}\nabla_\perp^2\right)A_0(\vec{x},t)+E-A_1^2(\vec{x},t)\right.\\ &\qquad\left.+\sqrt{\frac{2}{\gamma_0 n_{th}}}\,\xi_0(\vec{x},t)\right]\,, \qquad (1)\\ \frac{\partial}{\partial t}A_1(\vec{x},t) &= \gamma_1\left[-\left(1+\mathrm{i}\Delta_1-\mathrm{i}\nabla_\perp^2\right)A_1(\vec{x},t)+A_0(\vec{x},t)A_1^*(\vec{x},t)\right.\\ &\qquad\left.+\frac{1}{\sqrt{\gamma_0 n_{th}}}\,\xi_1(\vec{x},t)\right]\,, \qquad (2)\end{aligned}$$

where:

- γ_0 and γ_1 are the cavity damping rates for the pump and signal fields, respectively;
- the detuning parameters are defined as

  $$\Delta_0=\frac{\omega_0-2\omega_s}{\gamma_0}\qquad\qquad \Delta_1=\frac{\omega_1-\omega_s}{\gamma_1}\,, \qquad (3)$$

  for the signal and pump field, respectively, where ω_0 and ω_1 are the longitudinal cavity frequencies closest to $2\omega_s$ and ω_s, respectively;
- the transverse Laplacian

  $$\nabla_\perp^2=\frac{\partial^2}{\partial x^2}+\frac{\partial^2}{\partial y^2} \qquad (4)$$

  describes diffraction in the paraxial approximation. In the case of optical systems, diffraction together with nonlinearities is the very origin of spontaneous pattern formation, and plays a role similar to diffusion in nonlinear chemical reactions. Here x and y are dimensionless transverse coordinates, since we have scaled our space variables to the length

  $$l_d=\left(\frac{c^2}{2\omega_s\gamma_1}\right)^{1/2} \qquad (5)$$

  which represents the characteristic length for pattern formation in a OPO cavity;
- E is the scaled amplitude of the input field E_{in};
- the terms A_1^2 and $A_0A_1^*$ at r.h.s. of Eqs. (1), (2), respectively, describe the action of the nonlinear material;

#1968 - $10.00 US
Received June 25, 1997; Revised July 2, 1997

- $\xi_1(\vec{x},t)$, $\xi_0(\vec{x},t)$ are Langevin noise terms which describe quantum fluctuations. They have zero average, and the only nonvanishing correlation functions between them are:

$$\langle \xi_1^*(\vec{x},y)\,\xi_1(\vec{x}',t')\rangle = \langle \xi_0^*(\vec{x},y)\,\xi_0(\vec{x}',t')\rangle = \frac{1}{2}\delta(\vec{x}-\vec{x}')\delta(t-t')\,, \tag{6}$$

  so that noise is white both in space and in time;

- the parameter n_{th}, whose inverse measures the level of quantum noise, is given by:

$$n_{th} = \frac{\gamma_1^2}{g^2} l_d^2\,, \tag{7}$$

  where g is the coupling constant of the interaction between the two fields; this parameter represents the number of pump photon in the characteristic area l_d^2 which are needed to trigger the thresholdfor signal generation.

The semiclassical picture is obtained by dropping the noise terms ξ_0 and ξ_1 in Eqs. (1), (2). As shown in [8], in the case $\Delta_1 < 0$ the threshold of the OPO corresponds to

$$E_{th} = \sqrt{1+\Delta_0^2} \tag{8}$$

and immediately above threshold the OPO emits a signal field in the form of two plane waves with propagation direction symmetrically tilted with respect to the axis of the cavity. These two waves interfere with each other and give rise, in the near field, to a stripe or "roll" pattern, shown in Fig. 2a. The roll is the simplest spatial pattern that can spontaneously form in nature. In the far field, on the other hand, the two plane waves give rise to two localized spots (Fig. 2b). Although always symmetrical with respect to the origin, the position of the two spots can arbitrarily rotate around the origin; correspondingly the orientation of the rolls in the near field is arbitrary and depends only on initial conditions.

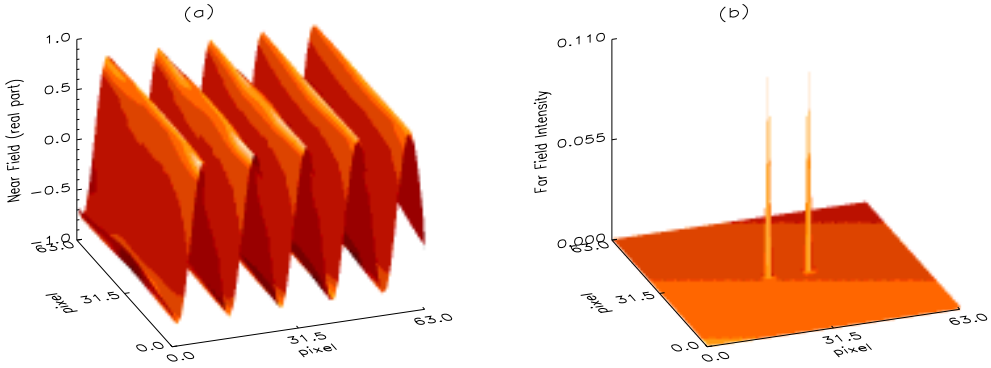

Fig. 2. Roll pattern. a)Near field distribution of the most amplified quadrature; b) far field intensity.

3. From below to above threshold

In the quantum description, as that given by Eqs. (1), (2) including the Langevin force terms, there are photons in the signal field even below threshold. As a matter of fact, it is well known that the degenerate OPO signal field below threshold is in a squeezed vacuum state; its spatial structure was analyzed in [9,4]. This means that below threshold the

#1968 - $10.00 US
Received June 25, 1997; Revised July 2, 1997

signal field is zero only on average. More important, as we show here, the signal field displays a spatial modulation with a noteworthy level of self–organisation. As a matter of fact, well below threshold the signal field is completely noisy both in the far and in the near field, and corresponds basically to a white noise configuration. However, as one gets closer to threshold it acquires an increasing level of spatial order [5].

A short animation (Fig. 3) shows the dynamics of the quantum images as the input field amplitude is gradually varied from below to above threshold. The scan of the threshold region is built up in the following way: by fixing the input field value, we let the system evolve until it reaches the regime. Actually this stage is quite long due to critical slowing down of fluctuations close to threshold. At this point we record the dynamics of the system at regime, by taking a few snapshots of the field distribution in the transverse plane, at time intervals of $3\gamma_1^{-1}$. Then, the input field amplitude is slightly increased, and the same procedure repeated. We do these steps for several increasing values of the input field, until the system is above the threshold.

The left panel in the animation shows the configuration of the most amplified quadrature component of the signal field $\mathrm{Re}A_1(\vec{x},t)$ in the near field, while the right panel displays the corresponding intensity distribution of the signal far field. What we see here is a stochastic realization of the dynamics of the system, obtained by numerically integrating Eqs. (1), (2) in a square with periodic boundary conditions; the numerical procedure is outlined in [5]. The far field distribution is obtained by Fourier transforming the near field. Parameters are chosen in such a way that the threshold corresponds to $E = \sqrt{2}$.
Starting from values of the input field below the threshold, we observe in the animation an irregular spot pattern in the near field.

Fig. 3. Click in the space to start the Quickmovie of the scan of the threshold region of the OPO obtained by varying the input field amplitude as shown in the bottom part of the animation. Parameters are $\gamma_1/\gamma_0 = 1$, $\Delta_0 = 1$, $\Delta_1 = -1$, $n_{th} = 200$. Threshold value of the input field is $E = \sqrt{2}$.

Due to the presence of noise, the spots perform a slow random walk in the transverse plane; as a consequence the signal field mean value vanishes everywhere. However, in a single snapshot, the distribution of spots over the transverse plane displays a clear spatial order, and the probability of finding two spots at a distance r apart has maxima when r is an integer multiple of the critical wavelength $2\pi/k_c$, which characterizes the modulation of the roll pattern above threshold. The far field intensity distribution appears to be concentrated on the critical circle of radius k_c. Over the far field circle, two couples of bright spots, opposite to each other with respect to the center of the circle, are clearly visible.

#1968 - $10.00 US Received June 25, 1997; Revised July 2, 1997

As the input field amplitude is increased across the threshold, the system undergoes a process of progressive coalescence of the spots into stripes, to approach a roll configuration as that shown by Fig. 2a. For quite a range of values of the input field the system is still "undecided" on which direction it should form them. Further on, beyond the threshold, the rotational symmetry is broken and rolls emerge in a definite direction; this is a priori arbitrary and, in the case of these numerical simulations, the system selects vertical rolls. Correspondingly, the two surviving spots in the far field pattern are aligned on the horizontal axis.

The animation shows the gradual transition from a quantum image (the spot pattern) below threshold, to a classical image (the roll pattern) above threshold. The far field intensity distribution shows correlated pair of maxima, in symmetrical position with respect to the center of the critical circle; this provides a spatial evidence of the mechanism of twin photon production. This feature, together with the analysis of spatial correlation between intensities fluctuations in the far field, gives evidence of the quantum nature of the fluctuations that originate the signal field [5,6].

4. An experimental approach to quantum images

The experiment, performed at the Optical Nonlinear Processes Laboratory in Como, concerns the characterization of the transverse intensity distribution of the parametric down–conversion generated by single pump pulses in a single nonlinear crystal, *via* travelling-wave parametric amplification of the vacuum-state fluctuation (the quantum noise).

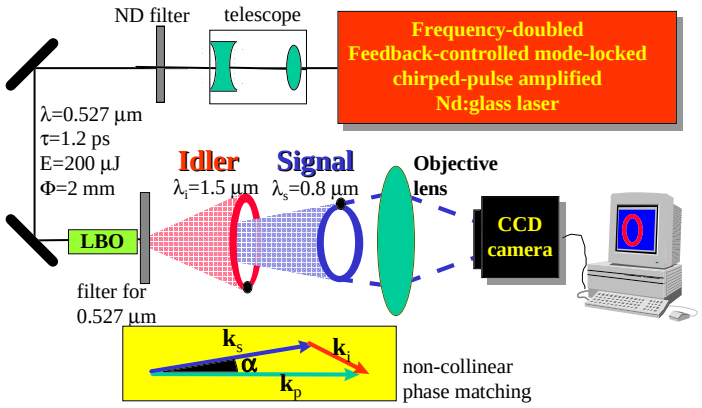

Fig. 4. Schematic lay out of the experimental set up. Parametric emission is accomplished by means of single pump pulses travelling in the LBO crystal. Signal and idler waves are preferentially generated along two cones, whose apertures fulfill the phase matching requirement. Far-field and near-field intensity distributions of the signal are detected by means of CCD camera and suitable objective optics.

The schematic lay out of the experimental set up is given in Fig. 4. The pump source is a frequency-doubled, feedback-controlled mode-locked, chirped-pulse amplified Nd:glass laser (model TWINKLE, produced by Light Conversion, Vilnius), delivering 1.2 ps single pulses at 527 nm, with transform-limited spectral bandwidth, energy up to 2.5 mJ and repetition rate of 2.5 Hz. The pulse energy and the beam diameter at the entrance of the non-linear crystal were set to about 0.2 mJ and 2 mm, respectively. At

#1968 - $10.00 US
Received June 25, 1997; Revised July 2, 1997

the corresponding intensity (about $4GW/cm^2$) the signal–idler emission is generated in our crystal in regime of linear amplification, i.e. with negligible pump depletion (below 1%).

The nonlinear crystal is a 15-mm long lithium triborate (LBO), cut for type 1 phase matching at $\theta = 90$ deg. and $\Phi = 11.6$ deg. For this cut, the ordinary polarized signal and idler beams exhibit a lateral walkoff of about 1 deg. respect to the extraordinary-polarized pump. Due to the relatively large beam diameter (with respect to the crystal length) we do not expect any relevant contribution of the lateral walkoff in our experiment. As far as the temporal walkoff (the group-velocity mismatch) is concerned, our pulse duration is also sufficiently large to make it ineffective in our experiment.

We detected the energy angular distribution of the parametric emission by means of a silicon CCD camera placed in the focal plane of a positive lens, behind the crystal (far field detection). Due to the cut off of the detector sensitivity at wavelengths larger than 1 μm only the signal wave was detected (here and in the following we arbitrary call signal and idler the shorter and longer wavelength components of the amplified noise, respectively). The near field energy distribution of the signal superfluorescence was obtained by imaging the exit face of the nonlinear crystal onto the CCD camera by means of suitable magnifying objective lenses. In both measurements the pump was eliminated by means of a low-band pass filter.

For a given crystal orientation, θ and Φ, with respect to the incident pump, we expect the parametric emission to occur at all angles (and wavelengths) which fulfill the phase-matching requirements (as previously mentioned, we do not expect any filter due to the spatial [11] or temporal [12] walkoff). The angular intensity distribution, however, does not exhibit a flat dependence on the signal-to-pump angle of non-collinear phase matching, α (see Fig. 4 for the definition): as it is evident from the single-shot angular spectrum in Fig. 5a, the signal emission is sharply peaked at a given α angle, whose value depends on the crystal orientation, θ and Φ.

Preliminary measurements lead us to attribute this behaviour to the peculiar features of the non-collinear tuning curves. In fact, for the given crystal orientation, the non collinear phase-matching angle α initially increases at shortening the signal wavelength from the collinear value ($\lambda_s \simeq 1\mu m$) toward the tuning edge ($\lambda_s \simeq 0.7\mu m$), it reaches a maximum value α_{max} for $\lambda_s \simeq 0.8\mu m$ and finally decreases back rapidly on approaching the very edge of the tuning. Therefore, we obtained a very large energy density just at $\alpha = \alpha_{max}$, due to the large number of wavelength which contribute to the emission in the same direction (the measured spectral bandwidth at $\alpha = \alpha_{max}$ is $\Delta\lambda_s \simeq 80nm$). Moreover, the fast drop of the detector sensitivity on going from $0.84\mu m$ to $1\mu m$ contributes in increasing the contrast between the ring and the inner part of the circle in Fig. 5a. Note that also the $0.76 - -0.7\mu m$ branch of the signal emission is not detected in Fig. 5a. In fact, it is also below the threshold of the detector sensitivity, being it distributed on a very broad range of α's.

The single-shot near-field intensity profile of the signal is presented in Fig. 5b, for the same crystal orientation and pump-pulse parameters as in Fig. 5a. From the figure it is evident the regular pattern structure (filamentation), whose details were changing from shot to shot (patterns are cancelled if averaged acquisition is taken). In agreement with our model, the characteristic spatial wavelength of this structure decreases when the crystal is rotated in order to get larger rings in the angular spectrum. In particular, from the 32 mrad half divergence shown in Fig. 5a one would expect a spatial wavelength of about $25\mu m$ in the pattern, in good agreement with the results shown in Fig. 5b.

#1968 - $10.00 US Received June 25, 1997; Revised July 2, 1997

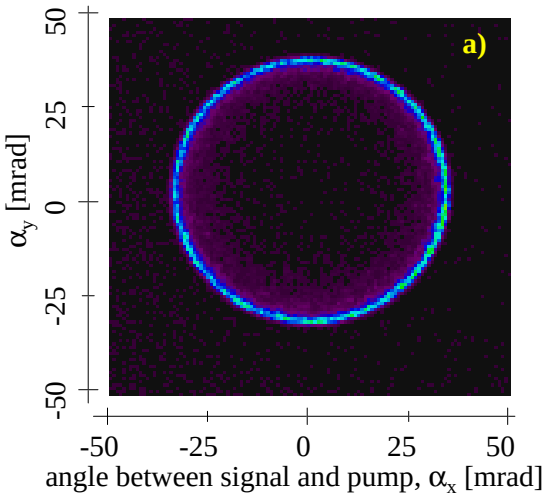

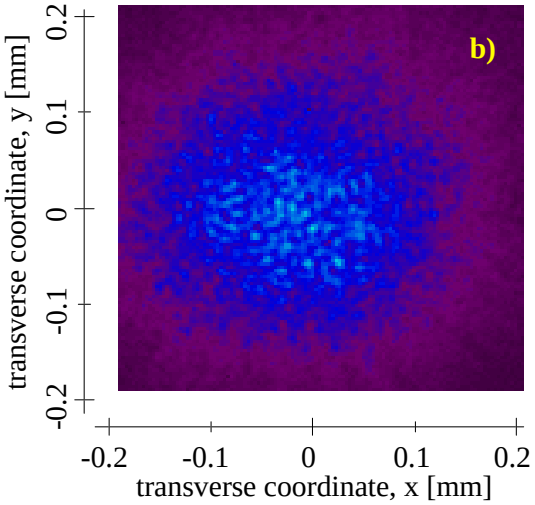

Fig. 5. a) Single-shot far-field intensity profile of the signal field. $\lambda_s = 0.8\mu m$, $\Delta\lambda_s = 80nm$ Crystal oriented for $\theta = 87^O$, $\Phi = 11.6^O$ b) Corresponding near-field intensity distribution.

Clearly there are important differences between the experiment and the theoretical model analysed in the previous sections. First of all, the experiment is performed in a pulsed configuration, while the model assumes a cw input. Second, the experiment is cavityless. Third the parametric down–conversion is nondegenerate, while the theoretical model assumes degeneracy. However, in both cases the patterns arise from a gain mechanism originated from parametric down-conversion. In the case of the OPO with optical resonator, analysed in the theory, the gain originates from the instability at the OPO threshold. In the experiment, the gain arises from the phase matching condition. A theory, formulated for a cavityless configuration, which leads to results qualitatively similar to those of the experiment, is the one which describes the onset of filamentation from quantum noise in propagation along $\chi^{(3)}$ media 10].

#1968 - $10.00 US
Received June 25, 1997; Revised July 2, 1997

Undoubtedly, there is a striking similarity between the experimental pictures and those obtained by numerical simulations of the quantum image dynamics, both in the near and in the far field. However, it must be noted, that the similarities concern only the classical aspects of the quantum image, in the sense that the same pictures could be generated by classical noise as well. In order to evidence unambiguous signatures of the quantum nature of fluctuations, as analysed in [6], one has to measure, in the far field, the spatial correlation function between intensity fluctuations of the signal and idler fields. This means that the experiment has to be performed in conditions such that both the idler field (red ring in Fig. 4) and the signal (blue ring in Fig. 4) are detected. The quantum nature of fluctuations is then shown by the fact the the maximum of correlation exists between opposite points on the two rings (the two black spots in Fig.4). Alternatively, the experiment can be realized in a degenerate configuration, as that assumed by the theory, in which only one ring is generated in the far field, and the maximal correlation arises between opposite points of the same ring [6]. These points are left for future investigations.

Acknowledgments

P. Di Trapani and A. Berzanskis acknowledge the Deutscher Akademischer Austauschdienst and the Vigoni-Programm 1997 for the financial support and give special thanks to Dr. W. Chinaglia for precious help in the experiment. G.-L. Oppo and R. Martin acknowledge EPSRC (grant K/70212) of the United Kingdom. This research was carried out in the framework of the activities of the Network QSTRUCT (Quantum Structures) of the TMR Program of the European Union.

#1968 - $10.00 US Received June 25, 1997; Revised July 2, 1997